Mathematical simulation of multiphase steelmaking reactions in the electric arc furnace

Rodolfo D. Morales[1)], M. Macias[1)], Ruben G. Lule[2)] and FranciscoLopez[2)]

1) Instituto Politécnico Nacional-ESIQIE, Dept. Metallurgy, Lindavista, Mexico D.F., CP 07338

2) Arcelor-Mittal Steel, Process Engineering Group, Lazaro Cardenas Michoacan. CP 60950

Abstract: A mathematical simulator for the electric arc furnace has been developed. The main characteristic of this simulator is the integration of all steelmaking reactions having place at the main interfaces in the electric arc furnace. These reaction-interfaces include metal-slag, gas-liquid, slag-carbon, carbon-gas and slag-gas and solid-gas involving, therefore, a complex multiphase system just as the steelmaking process actually is. Additionally, the present simulator has the capacity to model the kinetic behavior of the furnace as affected by intermittent operations such as feeding of lime, reduced iron pellets and oxygen lancing. The simulator is provided with a model to calculate the dynamic changes of physical properties of the slag and uses them to calculate slag foaming properties. The integration of slag foaming index into the kinetic equations makes possible to describe the dynamic foaming index which changes according to the specific operating conditions of the furnace. The capability of this simulator to predict the process dynamics of the electric arc furnace (EAF) was tested in current heats in a furnace with a capacity of 220 tons demonstrating an excellent agreement between the predicted and actual process kinetics. This simulator can be used on-line, for process control and off-line for process design purposes.

Keywords: EAF, mathematical simulator, molten slag, foaming, interfaces

1. Introduction

A mathematical simulator for EAF, melting scrap, was developed by Matson and Ramirez [1]. Other simplified models were reported by Fruehan [2].Kinetic models of steelmaking processes like BOF and EAF were developed by the group of the authors some years ago [3,4]. In these last two cases bath chemistry and temperature evolution with time are predicted reasonably well. Specifically, the EAF simulator was based on a set of differential equations involving mass balances and kinetic expressions. However, some empirical correlations obtained through data fitting of actual EAF operations were employed and integrated into the model. Just to give two examples, lime dissolution and pellets of direct reduced iron (DRI) were integrated in this simulator through correlated expressions. These expressions, because of their empirical nature, are far away from being descriptive of the phenomenology of steelmaking processes. The current trend of steelmaking research has provided new insights which can be used to avoid the empirical approaches and then is advisable to use this knowledge to improve former mathematical simulators. Therefore, the aim of the present work is to improve our mathematical simulator with updated phenomenological models available in the open literature. The final objective is to count on a simulator focused on the phenomenology of steelmaking processes, particularly, EAF steelmaking. The following lines describe, in a summarized way, the main features of this simulator and its corresponding application to a current EAF in the company Arcelor Mittal Steel located in Lázaro Cardenas Michoacán, Mexico, hereinafter called here AMLC.

2. Plant Description

Steelmaking facilities at AMLC consist of four EAF´s with a capacity, each one, of 220 tons of steel. These EAF´s are powered by 120 MW transformers delivering electric energy to the three electrodes. All furnaces are equipped with copper injection supersonic lances to supply oxygen and carbon powder to decarburize the melt and to foam slag. Steel is tapped through eccentric bottom tapping (EBT) system. DRI pellets are continuously feed through a hole on the roof. Materials like coke, lime and general fluxes can be fed also through that hole using an automatic electronically controlled system of transporting belts and hopers. A heal of liquid steel is left, from the precedent heat, to start the next heat charging scrap and feeding DRI pellets continuously at a rate governed by its metallization. Steel is later refined in three ladle furnaces and degasified in a vacuum degassed (VD) unit. Ultra low carbon steels are also refined in these facilities through a RHOB unit.

3. Mathematical Simulator

This simulator is divided in various mathematical models, each one dealing with different reactions and interfaces in a structure that allows each model to run independently to study specific phenomena. When all models are assembled then the simulator is ready to make predictions of process dynamics including all reactions at all interfaces. In the next lines each one of these models is described in a summarized scheme.

3.1 Static Model

To run a simulation first data, generated by a static model involving mass and energy balances, must be performed. This static model consists of a linear programming set of equations to find optimum charge policies of raw materials, mainly looking for the cheapest charge for a given heat or minimum possible energy consumption. The set of linear equations are derived from mass balances for metal and slag phases and energy balance of all steelmaking reactions. The SIMPLEX algorithm [5] is used to solve the system of linear equations to find out optimum points. All data generated by the static model are later used as initial boundary conditions to solve a set of differential equations describing the process dynamics. Therefore, initial slag chemistry is derived from this model and a thermodynamic model, to be described in the next section, start to calculate activities for all components in slag.

3.2 Thermodynamics for Multicomponent Slags

The kinetic expressions of this simulator require the knowledge of thermodynamic activities of steelmaking slags. Consequently, a thermodynamic model was developed to calculate those activities at each time step during the numerical integration of the differential equations. For this purpose the modified quasi-chemical model developed by Pelton and coworkers [6-8] was selected.

Basically, this model is based on the hypothesis that when a basic oxide mixes with a silicate slag, it promotes In order a decrease in the extent of de-polymerization due to the rupture of Si-O bonds according with the following reaction:

$$MO + (Si - O - Si) = Si - O - MO - Si \qquad (1)$$

This is equivalent to,

$$O^{2-} + O^0 = 2O^- \qquad (2)$$

Full de-polymerization occurs for a ratio MO/SiO_2=2, which corresponds to X_{SiO2} =1/3 being this the same composition corresponding to maximum ordering for silicate slags and is attributed to the formation of orthosilicate ions. The quasi-chemical model assumes that the atoms mix substitutionally on a quasi-lattice with a constant coordination number (z=2), forming, for a binary silicate slag the following pair of bonds: M-M, Si-Si and M-Si, where the energy change is dependent upon the local environment of the pair-bonds involved. Equation (2) can also be represented as a reaction expressing the different types of bonds in the binary silicate system ($MO-SiO_2$) as follows:

$$[M\text{-}M]+[Si\text{-}Si]=2[M\text{-}Si] \qquad (3)$$

[M-M] and [Si-Si] represent the two terms on the left side of Eq. [1], while [M-Si] represents the term on the right side of the same equation. A change in free energy in the previous reaction indicates a random distribution of M-Si bonds, while if the change in free energy is negative, then, the formation of pair-bonds M-Si is promoted, but if the change in free energy is positive, then, the formation of pair-bonds M-M and Si-Si is now predominant. Thus, in order to describe the thermodynamic properties of slags in the quasi-chemical model, the concentration of pair-bonds must be computed (X_{ij}). This is in fact, the major difference with the structural model since in such a model the free energy change is based on the concentration of oxygen ions. The expression representing the free energy change for reaction (3) is the following,

$$\Delta g_{mix} = \left(\frac{X_{M-Si}}{2}\right)(\omega) - TS^E = (\omega_{M-Si} - \eta_{M-Si}T) \qquad (4)$$

ω is the molar enthalpy change involved in Eq. [3], which is expressed in terms of pair-bond energies («M-Si), and η is the non-positional entropy change. When $(\omega_{M-Si} - \eta_{M-Si}T)$ is a negative, M-Si pairs predominate. The excess entropy (S^E) is the sum of positional and non-positional entropies. Equation (4) is then derived and equalized to zero to find out the minimum for concentrations of each pair of bonds.

3.3 Carbon-Gas and Carbon-Slag Interfaces

Figure 1a is scheme of the reaction interfaces in the steelmaking-multiphase system used in the construction of this simulator and Figure 1b shows an enlarged scheme of carbon-gas and carbon-slag interfaces. This model simulates the injection of carbon particles in the slag to control its oxidation level and maintaining the metallic yield. It is based on the work of Morales et al.[9]. Consists on an energy balance, the energy of the particles in the gaseous phase (E_p^g) of the energy of the particles in the gas phase is employed to overcome and interfacial resistance W, to displace a portion of the liquid slag in front of the interface due to the penetrations of the solid particles E_p^l and to maintain their own energy within the liquid slag, E_p^l. The energy balance is given by the following equation:

$$E_p^g = E_p^l + E_l^p + W \qquad (5)$$

This energy balance permits the calculation of fraction of solids that is able to pass through the gas-liquid interface and react with the liquid slag to reduce the iron oxide content through the reaction,

$$C + (FeO) = Fe + CO \quad (6)$$

However, the contact between carbon particles and the molten slag is not direct it takes place through the gas phase, this means that the solid particle remains in the core of a gas bubble and (FeO) reacts with CO to be reduced according to,

$$(FeO) + CO = Fe + CO_2 \quad (7)$$

CO_2 diffuses through the gas phase to react with the carbon particle, to rebuild the CO supply through the Boudouard´s reaction,

$$CO_2 + C = 2CO \quad (8)$$

Therefore reaction (6) is the overall reaction of two partial reactions (7) and (8).

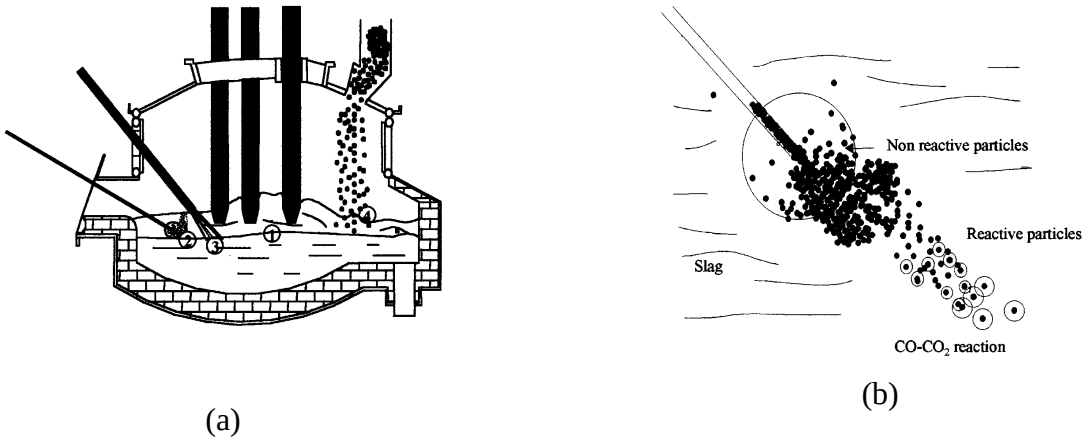

Fig. 1—(*a*) Chemical reaction subsystems: ① metal-slag interface, ② carbon-slag interface, ③ oxygen-slag-interface, and ④ DRI melting. (*b*) Closeup of the reaction mechanism for the reduction of iron oxide with carbon particles.

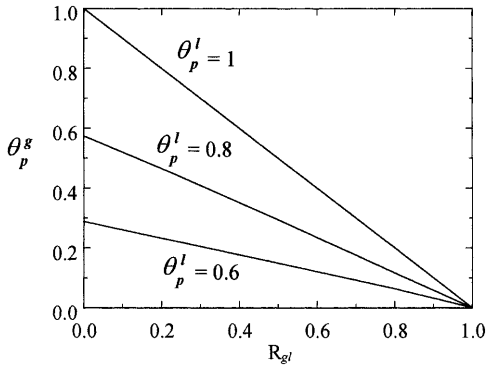

Fig. 2—Relationship between the volume fraction of particles that cross the gas-liquid slag interface and the volume fraction of particles.

The surface tension of steelmaking slags depends, evidently, on their chemistry being silica an active component that decreases this physical property. In other words, silicate molecules are adsorbed in the gas-liquid interface poisoning

the bubble available area for reaction avoiding the contact between the gas phase and slag at the gas-slag interface. To estimate the fraction of the available area of bubbles occupied by silicate molecules a Langmuir type equation for adsorption was used and using data of surface tension for slags [10] an expression linking this fraction with the slag chemistry was derived as follows:

$$\Theta_{SiO_2} = 0.3124 - 0.213\left(\frac{mass\ pct\ FeO}{100}\right) + 0.714a_{SiO_2}^2 \qquad (9)$$

With the thermodynamic model, described above, the silica activity in the molten slag can be calculated and its magnitude is substituted in equation (9) together with the mass % FeO calculated with the kinetic model making possible to know the occupied fraction. The fraction of particles that cross over the slag-gas interface Θ_p^g is plotted against the resistance to penetration given by the ration between the interface energy opposing penetration to the kinetic energy contained in the solid particles just before they penetrate this interface and is plotted in Figure 2. The fraction of solids unable to pass through the metal-slag interface is carried out by the gas toward the furnace exhausting system. The kinetic expression for iron oxide reduction with carbon particles is given by,

$$\frac{dW_{FeO}^{C_s}}{dt} = Q_s\Theta_p^g\frac{M_{FeO}}{M_C}\left[1-\left(\frac{r_{p(t)}^f}{r_0^p}\right)^3\right] \qquad (10)$$

Where $W_{FeO}^{C_s}$ is the mass of FeO reduced by carbon, t is time, M_{FeO} and M_C are the molecular weight and atomic weight of FeO and Carbon, Q_s is the mass flow rate of carbon particles $r_{p(t)}^f$ (calculated through a separated model as reprted in reference (4)) is the final size of a particle after a computing time step and is dependent on time. One example of numerical results of this model is given in Figure 3. There is seen that for a fixed flow rate of carrier gas of carbon particles reduction rate increases with mass flow arte of solids and decreases with silica activity as it is expected given the poisoning effects of this oxide. During injection of carbon in the EAF the simulator is informed with a size distribution curve of these particles and using a Monte Carlo simulation approach; the simulator chooses the size to be simulated at some given computing time step in a random fashion.

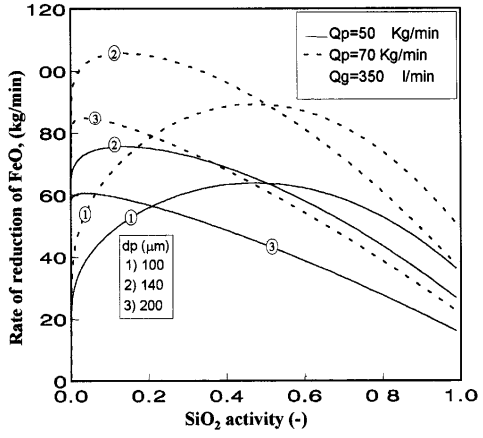

Fig. 3—Effect of silica activity on the rate of reduction of iron oxide for three different carbon particle sizes and two solid flow rates.

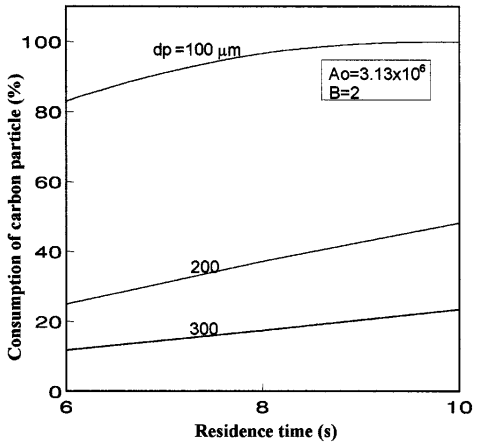

Fig. 4—Effect of residence time and carbon particle size on the consumption of carbon particles.

3.4 Solid-Liquid Interface, the Lime Dissolution Model

Dissolution mechanisms of lime in steelmaking slags are influenced by the chemistry of slag and limited by the saturation level of dicalcium silicate. In this work the lime dissolution model of Dogan et al. [11] is used, then the dynamic changes of lime weight is given by the equation,

$$\frac{dW_l}{dt} = \rho_L S \frac{dr}{dt} \qquad (11)$$

Where W_L is lime weight, r is lime particle radius, S is surface area of particle, k is mass transfer coefficient and n_L is number of lime particles, speed dissolution in equation (11) is calculated through the next equation,

$$-\frac{dr}{dt} = k\frac{\rho_s}{100\rho_L}\left[(\%CaO) - (\%CaO_{eq})\right] \qquad (12)$$

Where $(\%CaO)_{eq}$ is the solubility of CaO obtained from equilibrium diagram CaO-FeO-SiO_2. The mass transfer coefficient was calculated through a correlation for the Sherwood number given by,

$$Sh = 2 + 0.4\left[\frac{\varepsilon_{CO}\, d_p^4}{v_s^3}\right]^{\frac{1}{4}} Sc \qquad (13)$$

In this equation d_p is particle diameter and ε_{CO} is the stirring power generated by CO evolution from the steelmaking reaction and from the reduction reaction of iron oxide by carbon particles and is given by,

$$\varepsilon_{CO} = 14.2\frac{Q_{CO}T_s}{W_s} log\left(1 + \frac{hP_a}{1.46}\right) \qquad (14)$$

Where Q_{CO} is volume of CO evolved by the reactions and is calculated by the kinetic model, h is slag height, T_s is slag temperature, W_s is its weight and P_a is ambient pressure.

3.5 Metal-Slag Interface

Fruehan [2] and Sommerville [12] assume that reaction of decarburization at the metal-slag interface is carried out in two steps. In the first one carbon dissolved in molten metal reacts with CO_2 to produce CO and then CO reacts with FeO:

$$CO_2 + C(in\ metal) = 2CO \qquad (15)$$

The reaction of CO with FeO is the same as that in equation (7). The final expressions for the rate of consumption of FeO by the reaction reduction with carbon dissolved in the metal and the change rate of carbon dissolved in metal phase are given by the following expressions;

$$-\frac{d(pct\ FeO.W_s)}{dt} = M_{FeO}Ar^{"}_{CO} \qquad (16)$$

$$-\frac{d(pct\ C.W_m)}{dt} = M_C Ar^{"}_{CO_2} \qquad (17)$$

Rate reactions $r^{*}_{CO_2}$ and r^{*}_{CO} are calculated using the fraction coverage of this interface using equation (9) and the kinetic rate constants reported by Wei et al.[13].

3.6 Gas-Liquid Interface, Decarburization and FeO Formation by Oxygen

Chemical reactions for carbon and iron oxidations are represented as follows,

$$C + \frac{1}{2}O_2 = CO \qquad (18)$$

$$Fe + \frac{1}{2}O_2 = FeO \qquad (19)$$

If carbon concentration is high iron oxide is easily reduced as is accounted by Equation (16) and then the decarburization reaction is controlled by the supply rate of oxygen. If the carbon concentration in the metal is low then iron is oxidized and the decarburization reaction is controlled by mass transfer of carbon in the metallic phase. Therefore, decarburization kinetics was calculated using the expressions proposed by Matsuura et al. {14}, according to,

$$-\frac{d[Pct\ C]}{dt} = \frac{k_m A \rho}{W_M}[pct\ C] \qquad (20)$$

$$-\frac{d[pct\ C]}{dt} = \frac{Q_{O_2}\left(\frac{1000}{22.4}\right)(2 - R_{PC})0.012}{W_M}100 \qquad (21)$$

Where R_{PC} is the post-combustion ratio, k_m is the mass transfer coefficient, A is the interfacial area for reaction, ρ is melt density, W_M is its weight and Q_{O2} is the flow rate of oxygen blown through the lancing system. From industrial experience the critical carbon concentration for a shift from reaction control by rate of oxygen supply, equation (21) to mass transfer of carbon in the metals is smaller than 0.2%, equation (20).

3.7 Solid-Liquid Interface, Melting DRI Pellets in Bath

No being able, at the moment of writing this work, to build a reliable model for melting DRI pellets the former expression for DRI feeding rate as a function of metallization already published 4) was employed according to,

$$\frac{dW_{DR}}{dt} = -226403.57 + 5016.66(\%\ metallization) - 27.36(\%\ metallization)^2 \qquad (22)$$

3.8 Dynamic Foaming Index

Slag foaming is one of the most important operation in modern EAF steelmaking to assist in decreasing consumption of electric energy. Here a dynamic foaming index [4], based on the laboratory foaming index as defined by Ghag [15] is used here in order to follow variations of this important parameter with process time as a function of bath (metal and slag) chemistries and specific furnace operating conditions. The expression of this index is;

$$\Sigma_D = f_{r(t)}\Sigma \qquad (23)$$

Where Σis Ghag´s index and $f_{r(t)}$ is a time depending ratio of time depending volumes of gas in slag-gas emulsion and

slag according to,

$$f_{r(t)} = \frac{Q^{sl}_{g(t)}}{Q_{sl(t)}} \qquad (24)$$

The evolution of volume rate of gas in the slag-gas emulsion is given by,

$$Q^{sl}_{g(t)} = \frac{dV_{co}}{dt} + \frac{1}{[2460 + 18(mass\ pct\ FeO)]}\frac{dW_{sl}}{dt} \qquad (25)$$

$$Q_{sl(t)} = \frac{1}{[2460 + 18(mass\ pct\ FeO)]}\frac{dW_{sl}}{dt} \qquad (26)$$

All derivatives in equations (25) are calculated with the general kinetic model at each computing time step permitting the monitoring of the slag foaming time during the process time. Ghag´s laboratory data for foaming index corresponding to the CaO-SiO_2-FeO system were fitted through a polynomial expression according to;

$$\Sigma = -3.391X10^{-1}(\%CaO)^{-3.66} + 4.835X10^{-14} + (\%SiO_2)^{8.26} + 2.603X10^{-3}(\%FeO)^{1.318};\quad r^2 = 0.988 \quad (27)$$

3.9 Bath Temperature

Temperature of molten bath is computed based on a simplified relationship for the liquidus line from the Fe-C phase diagram adding a superheat of 100 K, according to,

$$T_b = 1908 - 88[\%C] \qquad (28)$$

At each carbon concentration, calculated through the general kinetic model, the bath temperature is calculated with the simple expression given in equation (28) and this temperature is used to calculate all slag and metal thermodynamics as well as all properties of gas, slag and metal phases. Slag viscosity was calculated using the Urbain model [16] and other physical slag properties were consulted in reference [17].

4. General Kinetic Model to Predict Dynamics of Steelmaking in EAF

All these models were assembled to build the general kinetic model which includes the kinetic expressions and mass balances for each oxide in slag and each component in molten metal. This model is summarized in Table I.

5. Results and Discussion

Figure 4 shows, for a given amount of particles, the percentages of particles consumed or reacted with iron oxide as function of the residence time in the slag phase. The smaller the particles are the more are consumed. Figures 5 and 6 show two simulations of two industrial heats employing different qualities of DRI pellets for a low metallization (87%) and high metallization (95%9, respectively. In these simulations carbon particle size is 250 μm. In both cases, the pattern of carbon and oxygen injection is as follows; Oxygen is injected from minute 10 until the end of the heat with a specific consumption of 10 Nm^3/ton of steel. Carbon particles are injected at minute 30 with a mass flow of 60 kg/minute and the flow rate of the carrier gas is 350 Nl/minute; this injection stops at minute 90. The dynamic foaming index (DFI) for both heats is also plotted in these figures too. The results with low DRI metallization indicate a much higher initial concentration of FeO as high as 43% compared with 20% for the case of High DRI metallization. Later,

the FeO concentration increases with injection of oxygen. This trend stops as soon as carbon injection starts; then, the concentration of FeO decreases continuously until it reaches a final concentration of FeO, at minute 90, of 30% and 10% for low and high DRI metallization, respectively. The DFI observed in these plots indicates two peaks, The first peak corresponding to the start time of oxygen injection indicating that this operation rises the slag foaming by, CO generation, for some time, after the effect decreases. That is, the injection of oxygen, produces large amounts of CO which foams the slag phase and the injection of carbon contributes also to the formation of larger amounts of CO. The minimum DFI is achieved at the end of the heat when the carbon injection stops. Comparing the DFI for both cases, higher DFI magnitudes are observed for the heat with lower DRI metallization with higher FeO concentrations. Iron oxide decreases the foaming index but apparently its reaction with carbon produces large amounts of CO to counteract the negative effects of FeO on slag foaming.

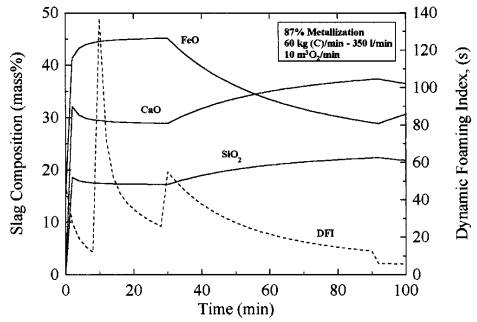

Fig. 5—Simulation of changes in slag chemistry and DFI during a hypothet- ical heat using a low metallization DRI.

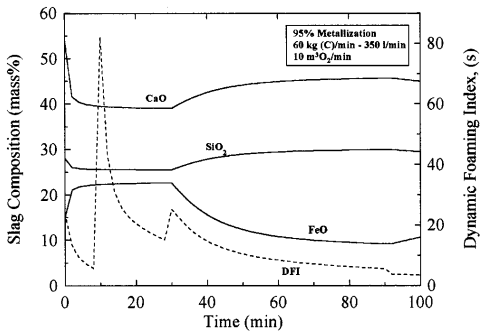

Fig. 6—Simulation of changes in slag chemistry and DFI during a hypothet- ical heat using a high metallization DRI.

The fact of using or not Monte Carlo simulation for reduction of iron oxide with carbon particles plays an important effect in predicting chemical changes of industrial slags. Indeed, Figure 7 show chemistry evolution of an industrial slag determined through the chemical analysis of samples taken from furnace number 4 at AMLC, using a fixed particle size of 250 μm (no Monte Carlo Simulation), which are fed at mass flow rate of 58 kg/minute with a flow rate of the carrier gas of 350 l/minute and DRI metallization of 90%. As is observed, ´predictions of the mathematical simulations and actual slag chemistry is excellent, as is always the case, when carbon concentrations fall down below 0.2% iron is oxidized to form iron oxide. The predictive capacity of this simulator was tested through the simulation of 15 heats and the relation between predicted slag chemistry, for each oxide in slag, and actual slag chemistry determined by chemical analysis is plotted in Figure 8. The mutual relation between each type of data is remarkably good indicating the very good capability of this simulator to predict reliably the dynamic behavior of actual heats. However, assuming a normal distribution of sizes for carbon particles going from 20 μm to 1000 μm introduced into the Monte Carlo simulator the predicted slag chemistry dynamics during carbon injection follow more irregular curves as is seen in Figure 9. Comparing with results presented in Figure 9 with those presented in Figure 7 is clearly seen that Monte Carlo simulations do not predict smooth curves for chemistry changes with time. Instead, chemistry curves yield irregular curves, particularly those corresponding to iron oxide, due to the random choosing procedure of particle size at each computing time step. Therefore, these type of predictions can be claimed to be closer to real furnace conditions.

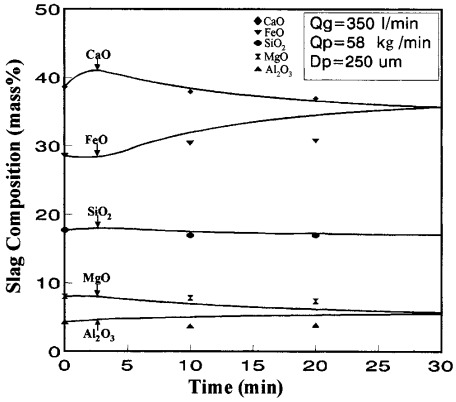

Fig. 7—Theoretical model predictions and comparison with industrial data on the chemical slag composition of the slag as a function of time, without Monte Carlo simulation.

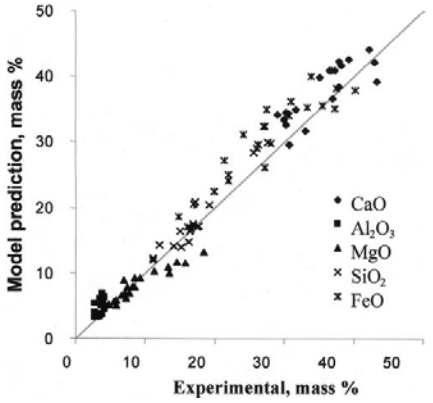

Fig. 8—Comparison between model predictions and industrial data on the chemical composition of slag for the whole set of heats studied.

Predictions of slag chemistry dynamics for a heat using DRI of very low metallization of 84-86% with a specific oxygen consumption rate of 3.7 m^3/ton of steel, lime consumption of 54 kg/ton of steel, injection of carbon particles with a mass flow rate of 3.18 kg/ton of steel are presented in Figure 10. FeO rises up to 42% during the first 35 minutes, when oxygen and carbon are injected simultaneously. The prediction of slag composition for CaO and SiO_2 are close to actual values, while in the case of FeO predictions during the 30 minutes of sampling are lower than the actual values. In spite of this the predicted final FeO concentration of FeO before tapping is closer to the actual concentration. The first and last analysis of FeO correspond to routine sampling, the first analysis is used by the furnace operator to establish the policy for oxygen injection.

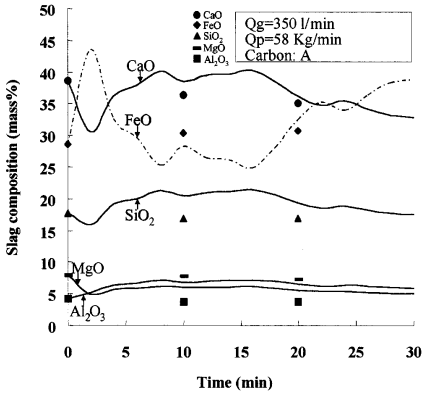

Fig. 9—Theoretical model predictions and comparison with industrial data on chemical composition of the slag as a function of time, using Monte Carlo method.

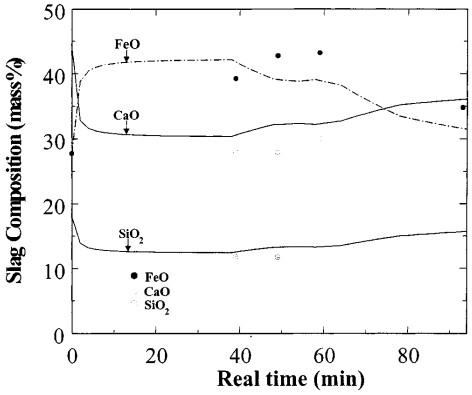

Fig. 10—Simulation changes of slag chemistry for an industrial heat (I). The points indicate experimental measurements of chemical composition of slag.

Predictions for another heat which used a DRI with a metallization of 91% was used, with a specific oxygen consumption rate of 50 kg/ton of liquid steel, a mass flow rate for injection of carbon equivalent to 30 kg/minute or 6.36 kg/ton of steel are presented in Figure 11. This heat starts and ends with lower concentrations of FeO compared with the previous heat because a higher DRI quality was melted. Nevertheless, it should be pointed out that the same results can be obtained through different process routes involving mainly procedure of carbon and oxygen injection and charging policies of lime and good DRI metallization does not ensure low final FeO contents and high metallic yields if the

ration between injections of oxygen and carbon are not properly balanced. DFI predictions are compared with the so called arc distortion. This parameter is a measure of the noise magnitude during the electrical arcing on the bath. As the arc distortion increases so does the magnitude of the noise, then, when slag foaming arises, both the distortion and the noise are smaller. Arc distortion is recorded from the panel control of the furnace and the corresponding data are stored in the process control computer. The complete different nature of the arc distortion makes difficult, if not impossible to achieve a full correlation between arc distortion between and DFI but their comparison must yield a qualitative agreement at least. To have the same trends between arc distortion and DFI, the fist is plotted as the reciprocal of arc distortion and compared directly with DFI in Figure 12. In this particular heat the DRI melted had a metallization of 91%, the mass flow of carbon was 65 kg/minute and the specific consumption of oxygen was 7.7 m^3/steel ton. The theoretical behavior of DFI indicates a slight foaming condition at the beginning of the hate decreasing steadily later on. At some certain time, after 20 minutes after starting there is magnitude peak of DFI. This trend of DFI corresponds very well to the actual reefing of this heat since at the beginning there is some amount of oxidized slag reacting with carbon in the melt making possible a moderate slag foaming. However, as fasr as carbon is not injected carbon the reaction stops and the slag foaming decreases. At minute 20 carbon and oxygen injections are applied inducing an intensive slag foaming well predicted by the appearance of the DFI peak. Close to the end of the heat a large CO evolution is predicted by the simulator, however, slag foaming decreases since oxidized slags have large density and smaller surface tensions decreasing the foaming capacity. The reciprocal of the arc distortion does not follow the exact path of DFI but it can be said that a qualitative agreement of the trends of these variables are the same. Therefore, it can be said that the present simulator has the capability for predicting slag foaming as dependent of furnace operation policies.

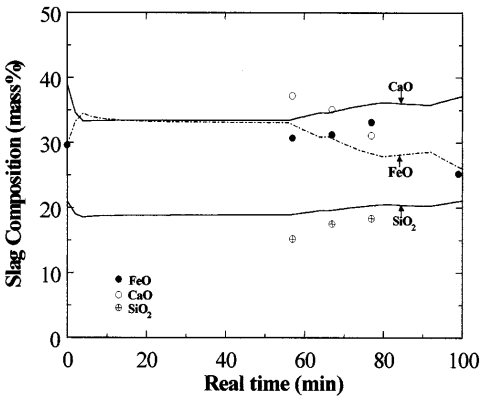

Fig. 11—Simulation of changes of slag chemistry for an industrial heat (II). The points indicate the experimental measurements of chemical compo- sition of slag.

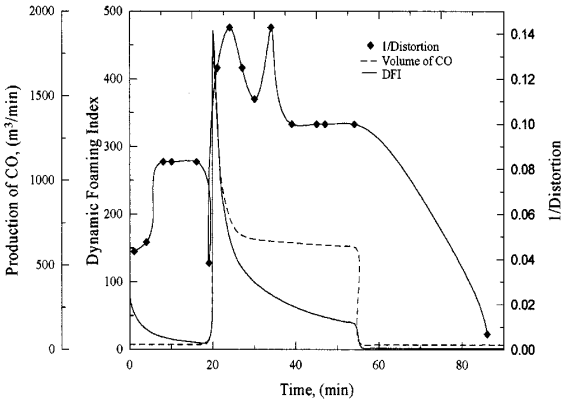

Fig. 12—Evolution of the dynamic foaming index in EAF steelmaking for an industrial heat compared with both the evolution of CO and actual 1/arc distortion.

Table IV. Overall Kinetic Model to Predict the Dynamics of Steelmaking in EAF

FeO	$\frac{d(X^{sl}_{FeO}\ W_{sl})}{dt} = \sum X^{DRI}_{FeO}\frac{dW_{DRI}}{dt} + \frac{M_{FeO}}{M_O}\sum K_{O_2}\ W_{O_2} - M_{FeO}\ A_{sm}\ r^{\circ}_{FeO} - Q_s u^g_p \frac{M_{FeO}}{M_C}\left[1 - \left(\frac{r^f_p}{r^o_p}\right)^3\right]$
CaO	$\frac{d(X^{sl}_{CaO}\ W_{sl})}{dt} = X^{lim\ e}_{CaO}\frac{dW_{lim\ e}}{dt} + d_{(t+t_{add})} + \sum\left[X^{DRI}_{CaO}\frac{dW_{DRI}}{dt}\right]$
SiO_2	$\frac{d(X^{sl}_{SiO_2}W_{sl})}{dt} = X^{lim\ e}_{SiO_2}\frac{dW_{lim\ e}}{dt} + d_{(t+t_{add})} + \sum\left[X^{DRI}_{SiO_2}\frac{dW_{DRI}}{dt}\right]$
MgO	$\frac{d(X^{sl}_{MgO}\ W_{sl})}{dt} = X^{lim\ e}_{MgO}\frac{dW_{lim\ e}}{dt} + d_{(t+t_{add})} + \sum\left[X^{DRI}_{MgO}\frac{dW_{DRI}}{dt}\right]$
Al_2O_3	$\frac{d(X^{sl}_{Al_2O_3}\ W_{sl})}{dt} = X^{lim\ e}_{Al_2O_3}\frac{dW_{lim\ e}}{dt} + d_{(t+t_{add})} + \sum\left[X^{DRI}_{Al_2O_3}\frac{dW_{DRI}}{dt}\right]$
Slag	$\frac{dW_{sl}}{dt} = \frac{d(X^{sl}_{FeO}\ W_{sl})}{dt} + \frac{d(X^{sl}_{CaO}\ W_{sl})}{dt} + \frac{d(X^{sl}_{SiO_2}\ W_{sl})}{dt} + \frac{d(X^{sl}_{MgO}\ W_{sl})}{dt} + \frac{d(X^{sl}_{Al_2O_3}\ W_{sl})}{dt}$
Carbon	$\frac{d(W^m_C)}{dt} = \sum\left[X^{DRI}_C\frac{dW_{DRI}}{dt}\right] - K_{O_2}\ W_{O_2} - M_C\ A_{sm}\ r^{\circ}_{FeO}$
Iron	$\frac{d(X^m_{Fe}\ W_m)}{dt} = X^{DRI}_{Fe}\frac{dW_{DRI}}{dt} + \frac{M_{Fe}}{M_{FeO}}(M_{FeO} + A_{sm} + r^{\circ}_{FeO} + r^{C(s)}_{FeO})$
Steel	$\frac{dW_m}{dt} = \frac{dX^m_C W_m}{dt} + \frac{dX^m_{Fe}W_m}{dt}$
Gas	$\frac{dW_{CO}}{dt} = \frac{M_{CO}}{M_C}\left[\frac{d(X^m_C\ W_m)}{dt}\right]$

Nomenclature:
X^j_i fraction of component i in phase j
K_{O_2} rate constant for the reaction of oxidation of liquid iron
m, sl metal, slag
DRI direct reduced iron
A_{ml} slag-metal interfacial area
M_i molecular mass of specie i
$r^{C(s)}_{FeO}$ heterogeneous rate of reduction of iron oxide due to carbon injection

Closing Remarks

The production of steel involves quite complex phenomena and understanding the mechanisms which lead to control them has been the driven force to improve EAF technology. There is a strong need to develop phenomenological models oriented to perform process control in order to achieve a more efficient use of global resources.

References

[1] S. Matson and W.F. Ramirez: Proc. 55th Electric Arc Furnace Conf., ISS; Warrendale PA, 1997, 675-685.

[2] R.J. Fruehan: Proc. Elliot Symp. On Chemical Process Metallurgy, ISS Warrendale PA, 1991, 1-10.

[3] P.G Garnica, R.D. Morales and N.U. Rodriguez: Proc. 77th Steelmaking Conf., ISS, Warrendale PA, 1994, 189-198.

[4] R.D. Morales, A.N. Conejo and H.H. Rodriguez: Metall and Mater, Trans. B, (2002) 33B, 187-199.

[5] G. Geiger: Direct Reduced Iron: Technology and Economics of Production and Use, R.L. Stephenson and R.P. Samailer Eds., TMS-AIME, Warrendale PA, 1980, 149-159.

[6] A.D. Pelton and M. Blander: Peroc. 2nd Symp. on Metallurgical Slags and Fluxes, TMS-AIME, Warrendale PA, 1984, 281-291.

[7] A.D. Pelton and M. Blander: Metall. Trans. B, 1986, 17B, 805-815.

[8] G. Eriksson and A.D. Pelton: Metall. Trans. B, 1993, 24B, 807-816.

[9] R.D. Morales, H. Rodriguez, P. Garnica and A. Romero: ISIJ Int. 1997, 37, 1072-1080.

[10] H.H. Rodriguez, A.N. Conejo and R.D. Morales: Steel Res., 2001, 72, 298-303.

[11] N. Dogan, G.A. Brooks and M.A. Rhamdhani: ISIJ Int., 2009, 49, 1472-1482.

[12] I.D. Somerville, P. Grievson and J. Taylor: Ironmaking and Steelmaing, 1980, 7, 25-31.

[13] P. Wei, M. Sano, M. Hirasawa and K. Mori: ISIJ Int., 1991, 31, 358-365.

[14] H.Matsuura, C.P. Manning, R.A. F. O. FORTES and R.J. Fruehan: ISIJ Int. 2008, 48, 1197-2105.

[15] S.S. Ghag, P.C. Hayes and H.G. Lee: ISIJ Int., 1998, 38, 1201-1207.

[16] K.C. Mills: Viscosities of Molten Slags, Verlag Stahleisen GmbH, Dusseldorf, 1995, 353.

[17] B.J. Keene and K.C. Mills: Physicochemical Properties of Slags, National Physical Laboratory, London, 1977.